LA-6397-MS
Informal Report

UC-20
Reporting Date: August 1976
Issued: August 1976

Plasma Experiments on the Scylla I-C Theta Pinch

by

Kenneth F. McKenna

los alamos
scientific laboratory
of the University of California
LOS ALAMOS, NEW MEXICO 87545

An Affirmative Action/Equal Opportunity Employer

UNITED STATES
ENERGY RESEARCH AND DEVELOPMENT ADMINISTRATION
CONTRACT W-7405-ENG. 36

Printed in the United States of America. Available from
National Technical Information Service
U.S. Department of Commerce
5285 Port Royal Road
Springfield, VA 22161
Price: Printed Copy $3.50 Microfiche $2.25

PLASMA EXPERIMENTS ON THE SCYLLA I-C THETA PINCH

by

Kenneth F. McKenna

ABSTRACT

Scylla I-C is a small scale (1-meter) research theta pinch developed for the experimental investigation of basic plasma physics processes and advanced concepts. The properties and stability characteristics of the Scylla I-C plasma, over a range of initial fill pressure from 100-500 mTorr D_2, are discussed in this report.

I. INTRODUCTION

The Scylla I-C linear theta pinch was constructed in order to provide a versatile research instrument to supplement the larger, less flexible theta-pinch programs. Small scale research studies and the experimental investigation of advanced concepts are carried out on Scylla I-C in order to provide basic physics information and diagnostic development for the present and future main theta-pinch efforts.

The Scylla I-C theta pinch is presently being used in conjunction with a high energy (~ 180 J) CO_2 laser to study the interaction of axially directed laser light with the dense ($n_e \sim 10^{17}$ cm^{-3}) theta-pinch plasma column.[1,2] The results of the laser-plasma interaction experiment will be presented in a later report. In the present report, the properties and stability characteristics of the high density Scylla I-C plasma are discussed; experiments were conducted over a range of fill pressures from 100-500 mTorr D_2. In a companion paper[3] the results of an investigation of plasma end-loss from the Scylla I-C plasma column are presented.

II. EXPERIMENTAL ARRANGEMENT AND DIAGNOSTICS

The geometry, energy storage capabilities, and electrical circuit parameters of the Scylla I-C theta pinch were determined from optimization studies intended to produce a dense ($n_e \geq 10^{17}$ cm^{-3}), low temperature plasma ($T_e \leq 50$ eV). A schematic of the theta pinch is shown in Fig. 1. Scylla I-C, constructed from Scyllac components, has a maximum capacitor energy storage of 175 kJ at 60-kV primary bank voltage. Fifty-four 1.8-μF capacitors feed the 100-cm long, 10.5-cm diameter single-turn compression coil. Primary bank operation at 40 kV generates a vacuum E_θ of 0.26 kV/cm at the inner wall of the 3.6-cm i.d. quartz discharge tube and a peak crowbarred compression field of 33 kG is obtained 2.0 μs after discharge initiation. The large coil diameter, in comparison with the discharge tube diameter, was used in order to obtain an effective crowbar of the main field discharge. Unless otherwise noted, the

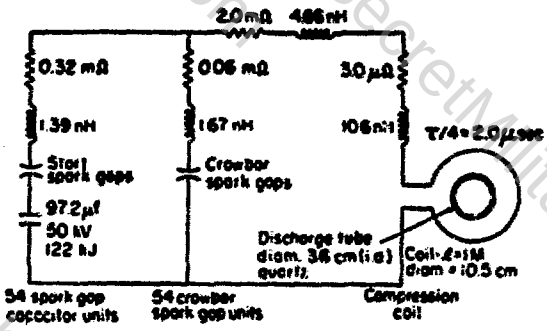

Fig. 1. Schematic of the Scylla I-C theta pinch.

plasma experiments discussed in this report were conducted at a primary bank voltage of 40 kV, over a range of fill pressure, P_0, from 100 mTorr to 430 mTorr D_2.

The principal plasma diagnostics consisted of external magnetic field probes, a laser interferometer and a plasma luminosity detector. The confining magnetic field waveform was measured with small induction coils placed near the outer wall of the discharge tube. Excluded flux measurements were made with a diamagnetic loop-probe system of standard design. The plasma electron density distribution was determined using an end-on 10-ns pulsed holographic ruby laser interferometer. A limited number of interferograms were taken with the ruby laser beam transverse to the plasma column. Side-on streak photographs of the Scylla I-C plasma column were taken with an Imacon camera unit focused on the coil midplane. In an attempt to identify plasma impurities, the spectrum of the theta-pinch plasma was obtained using a time integrated Hilger quartz prism spectrograph.

III. PLASMA PREIONIZATION STUDIES

Three different preionization systems were implemented on Scylla I-C in an attempt to optimize gas preionization. Initially, a single 0.1-uF capacitor was used as a gas preionizer in the theta-pinch mode. Experiments were conducted at capacitor charging voltages from 20 to 35 kV. This system was totally inadequate at high theta-pinch fill pressures ($P_0 \sim 300$ mTorr); at 100-mTorr fill, gas preionization with this unit was highly erratic, as indicated by the time of gas breakdown determined from the diamagnetic loop-probe response. Subsequently a 1.8-uF capacitor was installed, also in the theta-pinch preionization mode. Although this system was superior to the 0.1-uF capacitor unit, gas preionization remained irreproducible at the higher fill pressures.

The results of these experiments indicated that a more efficient coupling of the preionization system energy to the fill gas was required. Direct coupling was accomplished with a specially designed Z-pinch preionizer. The Z-pinch system consists of a 0.7-uF, 75-kV capacitor, a crowbar spark gap modified to accommodate five varistors, eight RG-14/59 load cables, and the Z-pinch electrodes. The Kovar-Pyrex electrodes were designed to fit flush with the outer diameter of the quartz discharge tube, allowing unhindered optical diagnostics of the plasma over the entire discharge tube cross section. The varistors were used to eliminate circuit ringing, thus producing a single, controlled pulse of input energy to the fill gas.

A schematic of the Z-pinch preionization system is presented in Fig. 2a. The ~ 4-us duration, 18-kA peak current waveform generated by this system at a capacitor voltage of 40 kV, is shown in Fig. 2b. A side-on streak camera photograph of the preionized plasma obtained with 100-mTorr fill pressure is presented in Fig. 2c. The Z-pinch current is of sufficient magnitude and rise time to cause pinching of the plasma under the $J_\theta B_r$ force interaction, as indicated on the streak photograph. At the termination of the pinched plasma column, the plasma expands and uniformly fills the discharge tube.

The density of the preionization plasma was determined from end-on ruby laser interferograms. A typical interferogram obtained during the pinch phase

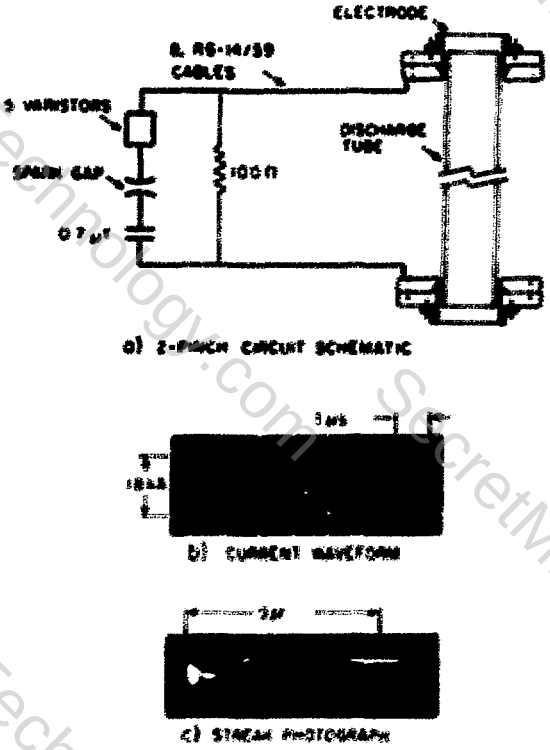

Fig. 2. Z-pinch preionization system: a) Z-pinch schematic, b) Z-pinch current waveform, c) side-on photograph of the preionization plasma.

with 100-mTorr pressure, is presented in Fig. 3. Spatial integration of the reduced density profiles indicated that for the 100-mTorr fill pressure case, 50% of the fill gas was ionized by the time the pinched plasma column had expanded to the discharge tube wall. For 500-mTorr fill pressure, about 20% of the gas was ionized at this time, t ≈ 2 μs. The primary bank discharge was initiated 10 μs after the preionization discharge.

IV. PREIONIZATION AND MAIN DISCHARGE PLASMA SPECTRA

Of primary concern when using a Z-pinch preionization system is the introduction of impurities, from the electrodes, into the main discharge plasma. To identify impurities in the plasma, the individual spectrums of the preionization and main discharge plasma were taken with an end-on viewing (through quartz windows) Hilger quartz prism spectrograph. Spectra were obtained with the 1.3-uF theta-pinch preionization system and the Z-pinch system with Heavy-Met (90% W, 6% Ni, 4% Cu) electrodes.

The spectrum of the preionization discharges shown in Fig. 4 was obtained at 100-mTorr fill pressure. The dominant spectral lines observed are from the deuterium Balmer series. The remaining identified lines are from excited carbon ions. No indication of Z-pinch electrode material line radiation can be found; the spectrum obtained with the theta-pinch preionization system is practically indistinguishable from that recorded with the Z-pinch system.

Spectra of the main plasma discharge at 40-kV primary bank voltage and 100-mTorr fill pressure are presented in Fig. 5. These data were taken with the same preionization systems as the results shown in Fig. 4. Other than the Balmer series, the identifiable lines result from carbon ion radiation. As in the case of the preionization plasma spectra, impurity radiation from the Z-pinch electrode material cannot be identified. Accordingly, the Z-pinch preionization system does not introduce undesirable perturbing effects into the main discharge plasma resulting from impurity contamination.

Fig. 3. Interferogram of the preionization plasma obtained with 100-mTorr fill pressure.

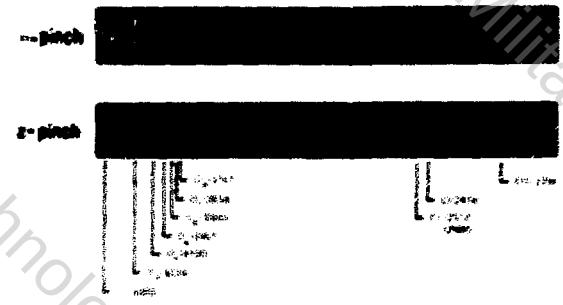

Fig. 4. Spectrum of the Scylla I-C preionization discharge.

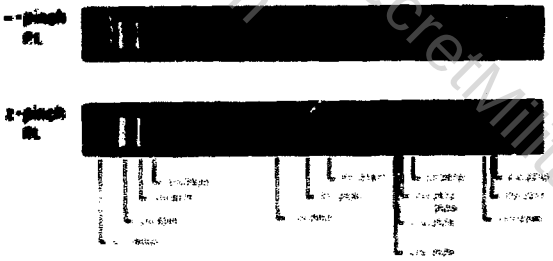

Fig. 5. Spectrum of the Scylla I-C main plasma discharge.

V. PLASMA COLUMN LUMINOSITY MEASUREMENTS

Streak camera photographs of the Scylla I-C primary discharge plasma column were made with the Imacon camera viewing the plasma side-on at the theta-pinch coil midplane. Figure 6a presents typical streak photographs at various camera sweep rates for 100-mTorr fill pressure. The slight bow evident on the streaks is not a plasma effect but results from disruption of the camera unit due to its close proximity to the theta-pinch coil and thus the primary discharge magnetic fields.

The dynamics of the plasma during the implosion and plasma column formation phase can be clearly identified from the fast sweep rate streaks where the initial radial shock wave and subsequent plasma oscillations are observed. The radial oscillations damp out approximately 1.3 μs after termination of the implosion. High frequency plasma oscillations have previously been observed[4,5] in high density ($P_o \geq 100$ mTorr) theta-pinch operation at the termination of the initial implosion. In this plasma regime, they are identified[4] as radial hydromagnetic oscillations of a cylindrical annulus of compressed plasma trapped between external and internal fields; such an annulus has been observed from end-on interferograms. Phenomenologically, at primary bank initiation the rapidly rising external magnetic field penetrates the preionized gas before the current sheath is completely developed and this field, which has leaked into the gas, is subsequently trapped and compressed by the imploding current sheath. At the termination of the initial implosion the plasma is contained within the annulus separating the external and compressed internal fields and oscillates about an equilibrium radius.

Assuming all the initial fill gas is swept up during the implosion, the equation of motion of the plasma annulus can be solved[4] yielding an oscillation period given by

a. Various Streak Camera Sweep Rates 100 m torr Fill Pressure

b. Various D_2 Fill Pressures

Fig. 6. Streak photographs of the Scylla I-C plasma column obtained at different camera sweep rates and initial theta-pinch fill pressures.

$$\tau_{osc} = 2\pi\sqrt{\frac{Nm_i}{B^2}} \quad , \qquad (1)$$

where N is the line density of ions of mass m_i in the annulus, and B is the external magnetic field. Considering the 100-mTorr fill pressure case, the period of the first oscillation, after the implosion, is about 220 ns and the average external magnetic field strength over this time interval $\sim$ 13 kG. With this value of magnetic field and $N = n_o \pi b^2 = 7.1 \times 10^{16}$ cm^{-1} (b is the discharge tube radius), Eq. (1) predicts an oscillation period of 235 ns, in very good agreement with the experimental result. The experimentally observed periods of the two successive oscillations are 160 and 130 ns respectively and the corresponding analytical values are 150 and 100 ns. Accordingly, it does appear that the radial oscillations of the dense plasma column observed in Scylla I-C are consistent with the theory of field trapping during the implosion phase.

Damping of the radial oscillations can be attributed to resistive field diffusion through the plasma. Neglecting convective effects, the diffusion equation can be written in one dimension as

$$\frac{\partial B}{\partial t} = \frac{c^2}{4\pi\sigma}\frac{\partial^2 B}{\partial x^2} \quad , \qquad (2)$$

where σ is the plasma conductivity and x is the coordinate perpendicular to B. The one-dimensional approximation overestimates the diffusion time since diffusion occurs more rapidly in cylindrical geometry. The characteristic time over which the magnetic field diffuses is, from Eq. (2),

$$\tau_{diff} = \frac{4\pi\sigma L^2}{c^2} \quad , \qquad (3)$$

where the diffusion length scale, L, can be taken as half the plasma radius $L = r_p/2$. From Spitzer[6] the plasma conductivity is given by

$$\sigma = 1.8 \times 10^{14}\frac{T_e^{3/2}}{\ell n\,\Omega} \quad , \qquad (4)$$

where T_e is in eV. The electron temperature, T_e, at the end of the implosion can be estimated by adapting a snowplow model for the implosion dynamics. In this model the ions are assumed to gain equal kinetic and thermal energies during the implosion while the electrons retain their initial preionization temperature; ohmic heating of the electrons is assumed small. At the termination of the implosion the ions rapidly transfer energy to the electrons, via collisions, until temperature equilibration is obtained. The ion energy at the end of the implosion is then $3/2\ kT = 2(1/2\ m_i v_i^2)$, where v_i is the inward radial velocity of the ions. Estimating the pinch time from the streak photographs to be $t_p \simeq 330$ ns (again for P_o = 100 mTorr) and taking $v_i \simeq b/t_p$, the kinetic temperature of the ions before energy equipartition with the electrons is approximately 40 eV. Thus, after temperature equilibration the electron temperature is about 20 eV. Over the damping time of the radial oscillations the plasma is compressed by the rising main magnetic field so that the electron temperature will increase over this time interval. Using the 20-eV electron temperature estimated above will thus set a lower limit on the calculated magnetic field diffusion time. Taking $\ell n\,\Omega \simeq 8$, $T_e \simeq 20$ eV and $r_p \simeq 0.6$ cm (obtained from end-on interferograms to be discussed), the estimated diffusion time is about 2.5 us, in reasonable agreement with the observed damping time of the oscillations, 1.3 us.

From the streak photographs of Fig. 6, the compressed plasma column is observed to be highly stable and reproducible for a period of approximately 8.5 us; after this time an m=2 instability is observed. The time required for an Alfvén wave to propagate from the theta-pinch ends to the midplane is about equal to the onset time of the m=2 instability, indicating that the instability may be a result of plasma rotation induced by end-shorting of the plasma radial electric fields.[7,8] The plasma column stability characteristics remain the same over a wide range of initial fill pressures (100-500 mTorr) as demonstrated in Fig. 6b.

VI. PLASMA DENSITY MEASUREMENTS

The time and spatial evolution of the main discharge plasma density distribution was determined with the ruby laser interferometer in an end-on single-

pass configuration. Figure 7 presents a time sequence of plasma column interferograms obtained for 100-mTorr fill pressure. The straight background fringe pattern was generated on each interferogram by a small angular deviation of the scene beam introduced between exposures taken with and without plasma. Plasma electron refractivity results in displacement of the background fringes, with one fringe displacement corresponding to a change in $\int n_e d\ell$ of

$$\Delta \int n_e d\ell = 3.24 \times 10^{17} \text{ electrons cm}^{-2} . \quad (5)$$

Each interferogram of Fig. 7 was obtained from a separate plasma discharge and the entire 3.8-cm diameter of the discharge tube was illuminated by the interferometer laser light.

The plasma column formation phase (t=0.5 μs, Fig. 7) is dominated by high m-number (m>6) flutes, with some of the flutes extending from the plasma column to the discharge tube wall. The annular distribution of plasma density, previously indicated to be a result of trapped magnetic fields, is observed during the early stages of the column formation phase. At later times, the plasma loses its annular structure through field diffusion, the flutes disappear, and a well confined high density plasma column is observed for several microseconds. The beginning

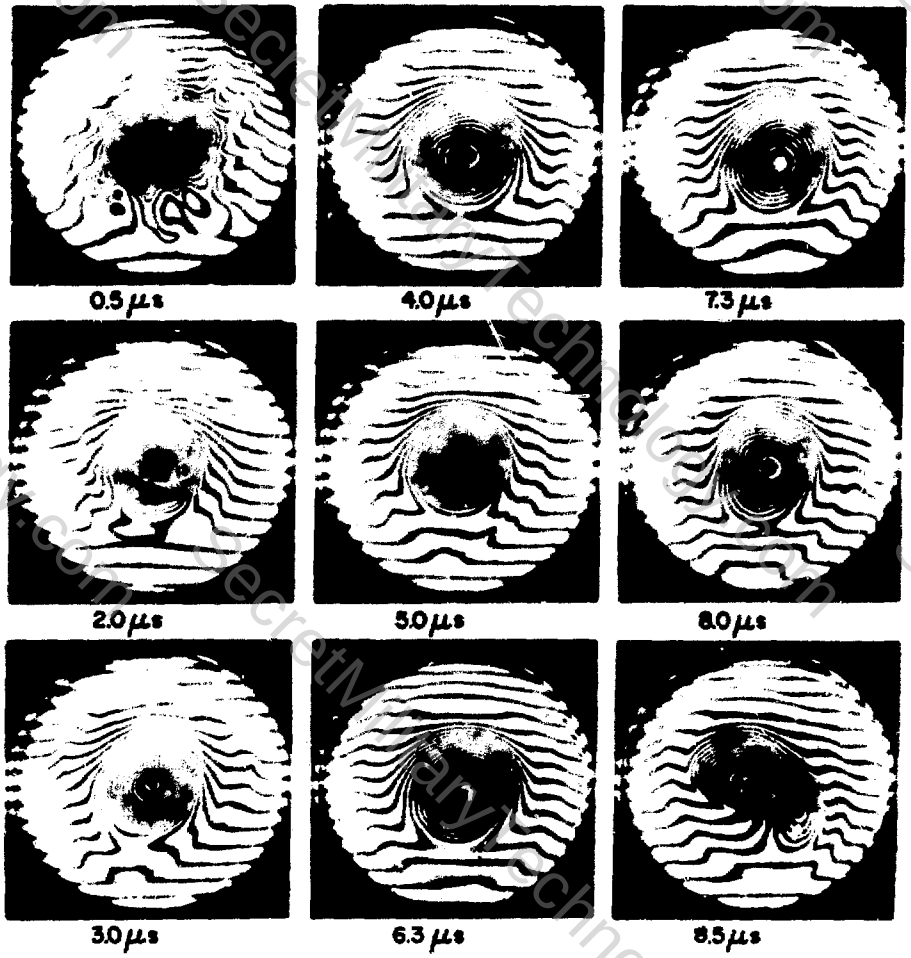

Fig. 7. Time sequence of plasma column interferograms obtained at 100-mTorr fill pressure.

of the plasma column breakup and filamentation (m=2) is evidenced at $t \geq 8.5$ μs.

Figure 8a presents a plasma column interferogram taken at $t = 2.7$ μs for a fill pressure of 300 mTorr and is typical of the high fill pressure data. The plasma electron density profile, derived from the interferogram of Fig. 8a is shown in Fig. 8b. The density profile deviates from a Gaussian, exhibiting a long tail which, at high fill pressures, extends to the discharge tube wall. Extracting exact plasma profiles from the interferograms taken at fill pressures greater than 300 mTorr is difficult due to the large number of closely spaced fringes. At $P_o = 500$ mTorr the total number of fringes was ≈ 77 at maximum compression, $t = 2.0$ μs. The peak density on axis could be estimated from simple fringe counting and the peak density determined from the end-on interferograms at 500 mTorr agreed within 20% with the values derived from a limited number of side-on interferograms.

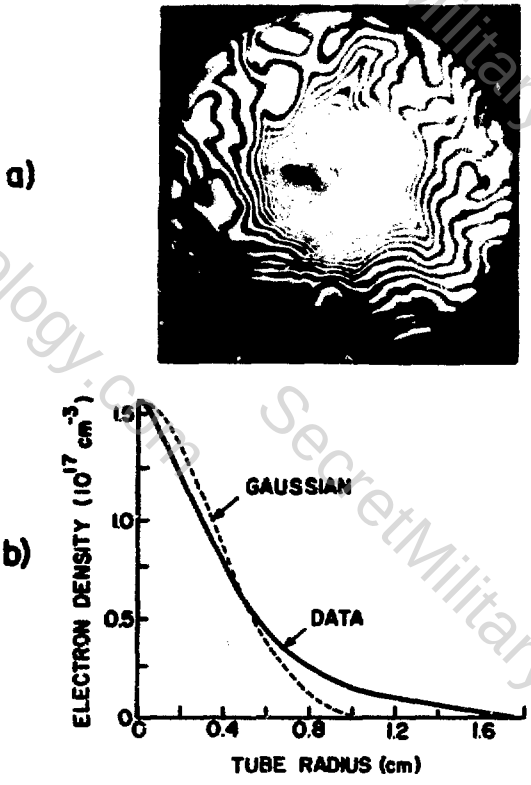

Fig. 8. Plasma column interferogram and reduced density profile for $P_0 = 300$ mTorr, $t = 2.7$ μs.

From the analysis of many interferograms, the average plasma density at maximum compression, $t = 2.0$ μs, was estimated to be $\sim 1.1 \times 10^{17}$ cm^{-3} at $P_o = 100$ mTorr, $\sim 1.5 \times 10^{17}$ cm^{-3} at $P_o = 250$ mTorr, and $\sim 2.3 \times 10^{17}$ cm^{-3} at 500-mTorr fill. Spatial integration over the reduced density profiles obtained at 100-mTorr and 250-mTorr fill, indicated that all of the fill gas was ionized and contained within the observable plasma density distribution at the time of maximum compression; only 70% ionization and containment was indicated from both end-on and side-on data at $P_o = 500$ mTorr.

In an attempt to generate a density minimum on the plasma column axis, and thus provide a "light pipe" for the CO_2 laser beam in the laser-plasma interaction experiment,[1] a forward bias field was applied. The bias field had a quarter cycle time of approximately 23 μs and a magnitude of ~ 1.8 kG at the time of primary bank initiation.

End-on interferograms taken at $t = 1.0$ μs with and without the applied bias field, for 100-mTorr fill pressure are presented in Fig. 9. A well defined density minimum on axis results when the bias field is applied. Density minimums could not be identified for fill pressures greater than 300 mTorr. At 100-mTorr fill, the minimum persists for a period of approximately 3 μs, its duration being limited by magnetic field diffusion. An estimate of the plasma column temperature can be made from the known diffusion time and the plasma radial dimensions determined from the interfergram of Fig. 9b. Solving for T_e by combining Eqs. (3) and (4), and taking $\tau_{diff} \approx 3$ μs, $r_p/2 \approx 0.45$ cm, and $\ln \Omega \approx 8$, an electron temperature of about 13 eV is determined for the observed plasma at $t = 1$ μs. Comparing this value with the estimated electron temperature at the end of the implosion $T_e \approx 20$ eV at $t_p \approx 0.3$ μs, obtained without forward bias for $P_o = 100$ mTorr, indicates that the bias field significantly reduces the electron temperature. Such a result is expected since the presence of the bias field decreases the inward radial velocity of the ions during the implosion thus decreasing the total ion energy at the termination of the implosion phase. In addition to a drop

in electron temperature, the peak plasma density decreases when the bias field is applied; at $t = 1$ μs, $n_e \simeq 1 \times 10^{17}$ cm^{-3} without bias and $n_e \simeq 0.6 \times 10^{17}$ cm^{-3} with bias, assuming a plasma column length of 100 cm. Since the main magnetic field, B, is independent of applied bias and $2nkT_e = \beta B^2/8\pi$, in the Scylla I-C plasma, the plasma β also decreases significantly when the bias field is applied.

VII. PLASMA EXCLUDED FLUX MEASUREMENTS

The effective radius r_{eff} at which magnetic flux is excluded from the compressed plasma was determined from diamagnetic loop-probe measurements. The excluded flux data, when appropriately combined with the known plasma density distribution, are used to determine the plasma β (ratio of plasma pressure to magnetic field pressure). From the β measurement an estimate of the plasma kinetic temperature can be obtained.

The diamagnetic loop-probe system consists of two closely spaced, magnetic pick-ups. A small magnetic probe ($NA \sim 0.3$ cm^2) measures the changing magnetic flux just outside the discharge tube and, since the probe area is fixed, the integrated signal gives the magnetic field external to the plasma. A single-turn loop encircling the discharge tube responds to the changing magnetic flux inside the discharge tube and therefore measures the magnetic flux excluded by the plasma. The signals from the loop and probe are nulled in the absence of plasma by means of a passive differencing circuit. The integrated difference signal is divided by the integrated probe signal to give the net flux excluded by the plasma. From this measurement the effective cross-sectional area of plasma from which magnetic flux is completely excluded can be determined. The diamagnetic loop-probe system was calibrated with a copper rod of known diameter which was inserted into the discharge tube and simulates the plasma column.

Four loop-probe systems were arranged along the axis of the discharge tube. Only the results obtained from the system located at the coil midplane will be discussed here; the axial variation of excluded flux is detailed in the companion report[3] which discusses the Scylla I-C end-loss experiments. The excluded flux radius derived from the loop-probe data taken at the coil midplane with 100-mTorr fill pressure is presented in Fig. 10. The implosion phase, damped oscillation phase and quiescent plasma column phase observed in the streak photographs can also be identified from the time history of the excluded flux radius. The excluded flux data of Fig. 10 are typical of those obtained at higher fill pressues. The relatively constant minimum value of r_{eff}, 0.22 cm, between ~ 1.5 and ~ 2.5 μs is nearly insensitive to fill pressure, changing only 15% between 100-mTorr fill (0.22 cm) and 500-mTorr fill (0.19 cm).

a) Without Bias Field

b) With Bias Field

Fig. 9. Plasma column interferograms taken with and without an applied bias field.

VIII. DETERMINATION OF PLASMA β

From the definitions of excluded flux and the pressure balance equation it can be shown[9] that the area of excluded flux, πr_{eff}^2, is related to the plasma β through the expression

$$\pi r_{eff}^2 = \int_0^\infty \left[1-\sqrt{1-\beta(r)}\right] 2\pi r dr \quad . \tag{6}$$

Assuming that the plasma temperature is independent of radius, pressure balance yields

$$\beta(r) = \frac{n(r)}{n_A}\ \beta_A \quad . \tag{7}$$

where n_A and β_A are the plasma density and β on axis. For a Gaussian density distribution, substitution of Eq. (7) into Eq. (6) yields an exact solution for β_A as a function of r_{eff} and the 1/e plasma radius. For a non-Gaussian profile such as shown in Fig. 8b, $n(r)/n_A$ must be determined graphically and the result substituted into Eq. (6) which can then be numerically integrated to determine β_A.

For the Scylla I-C density profiles at maximum compression, $t = 2.0$ μs, the β_A determined by numerical techniques were: $\beta_A = 0.44$ with $P_o = 100$ mTorr and $\beta_A = 0.33$ with $P_o = 250$ mTorr. The value of β_A obtained assuming a Gaussian density profile and calculating the 1/e radius using the peak density value were: $\beta_A = 0.63$ for 100-mTorr fill and $\beta_A = 0.37$ for 250-mTorr fill. The difference between the β_A determined numerically and that calculated assuming a Gaussian profile decreases as the fill pressure increases, being ∿ 29% at 100 mTorr and 11% at 250 mTorr. The convergence of the β_A values generated by the two techniques indicates that the density profiles more closely approximate a Gaussian shape as the fill pressure is increased. Assuming that the profile at $P_o = 500$ mTorr is Gaussian, the calculated β_A is then ≈ 0.17.

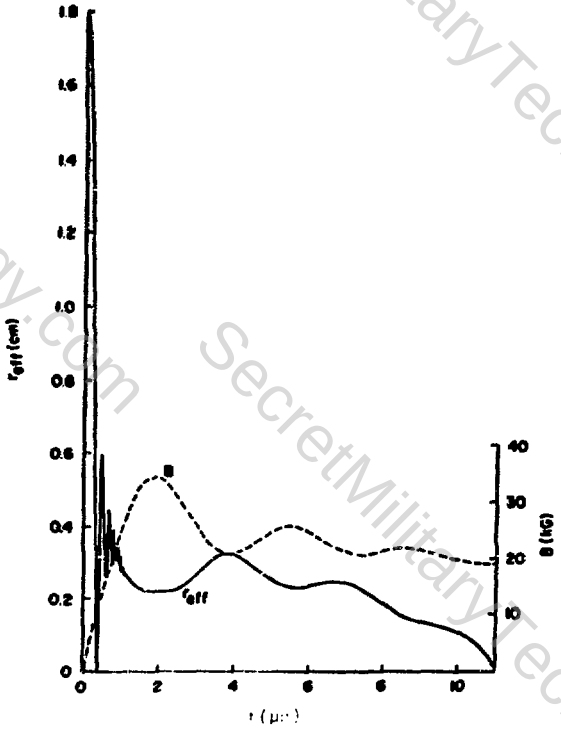

Fig. 10. Excluded flux radius obtained at 100-mTorr fill pressure.

IX. DETERMINATION OF PLASMA ELECTRON TEMPERATURE

The compressed plasma temperature is determined from the measured values of plasma density on axis n_A, the measured external magnetic field B, and the calculated values of β_A. From pressure balance,

$$\beta_A \frac{B^2}{8\pi} = n_A k(T_e+T_i) \quad . \tag{8}$$

In the high density plasma column the thermal equilibration time between electrons and ions is small ($\ll 1$ μs) so that $k(T_e+T_i) \simeq 2kT_e$. The plasma electron temperature can then be determined directly from Eq. (8).

X. SCYLLA I-C PLASMA PARAMETERS AND SCALING

Figure 11 summarizes the Scylla I-C plasma parameters n_A, T_e, and β_A obtained at maximum compression over the investigated range of fill pressure, P_o, from 100 mTorr to 500 mTorr. The error bars displayed on the plasma density data reflect the assumed uncertainty in the data reduction and indicate the error associated with the calculated value of T_e and β_A.

With the large variation in plasma β observed over the investigated range of fill pressures, it is difficult to analytically derive expressions which predict the scaling of the plasma parameters with fill pressure. However, empirical relations can be obtained from the data presented in Fig. 11. Accordingly, in the Scylla I-C theta pinch with constant discharge tube and coil diameters and constant E_θ and B, the plasma temperature $T_e = T_i \propto P_o^{-1}$, the

plasma density $n_A \propto P_o^{1/2}$ and the plasma $\beta_A \propto P_o^{-3/5}$, at the time of magnetic field maximum, t = 2.0 μs.

XI. PLASMA PARAMETERS WITH A 5-CM DIAMETER THETA-PINCH COIL

The previously discussed plasma experiments were conducted with a 10.5-cm diameter theta-pinch coil. In order to investigate the plasma parameters at a higher initial E_θ and peak magnetic field strength, the coil diameter was reduced to 5 cm. A less effective crowbar of the main field was obtained with the smaller diameter coil and only the plasma properties at peak field, prior to crowbar initiation, will be discussed here. The experiments were carried out at 40-kV primary bank voltage which produced a peak field of 46 kG, with a quarter cycle time of 1.4 μs, and an initial E_θ of 0.46 kV/cm at the discharge tube inner wall.

Plasma interferograms, obtained with the 5-cm diameter coil, showed physical features identical to those taken with larger bore coil; the plasma formation phase exhibited flute-like instabilities which disappeared in about 1 μs. The plasma column was well defined and of high density. The peak plasma density on axis was estimated, for 100-mTorr fill pressure data, from fringe counting. At fill pressures above 100 mTorr the plasma density was too high to be resolved by the end-on interferograms. For 100-mTorr fill, the peak plasma density $n_A \simeq 1.5 \times 10^{17}$ cm^{-3} at t ∿ 1.1 μs, slightly prior to peak field. The plasma β_A was determined as discussed above and found to obtain a peak value of ∿ 0.63. The plasma temperature, estimated from pressure balance, obtained a maximum value of ∿ 100 eV at t ∿ 1.1 μs. Assuming that the plasma parameters scale in the same manner in both theta-pinch coils, a peak density of 3.2×10^{17} with a corresponding electron temperature of 17 eV and β_A of 0.24 is indicated for the 500-mTorr fill pressure case.

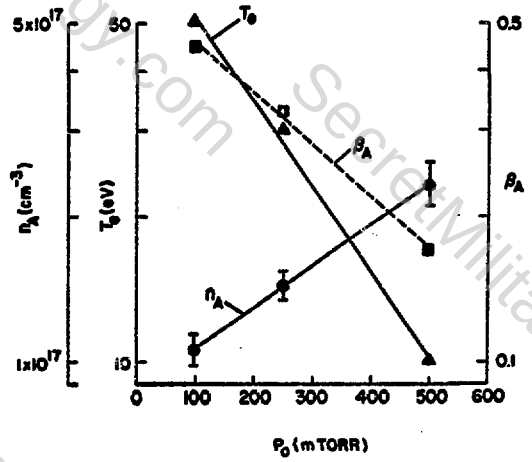

Fig. 11. Scylla I-C plasma parameters at the time of maximum compression, t = 2.0 μs.

In the Scylla I-C laser-plasma experiment[1] the inverse bremsstrahlung absorption length, ℓ_{ab}, is a fundamental parameter. For CO_2 laser radiation ℓ_{ab} can be expressed as

$$\ell_{ab} = \frac{1.03 \times 10^{35} (T_e)^{3/2}}{n_e^2 \ell n(1.39\, T_e)^{3/2}} \times \left(1 - \frac{n_e}{10^{19}}\right)^{1/2} \text{cm}, \qquad (9)$$

where n_e is in cm^{-3} and T_e in eV. Considering the 100-mTorr fill pressure data, the absorption length for the plasma parameters obtained with the 10.5-cm diameter coil, ℓ_{ab} = 612 cm, is slightly smaller than that indicated for the 5-cm diameter coil, ℓ_{ab} = 657 cm; at 500-mTorr fill pressure $\ell_{ab} \simeq 14$ cm for both coil configurations. Accordingly, in the Scylla I-C theta pinch significant changes in the inverse bremsstrahlung absorption length could not be produced by reducing the theta-pinch coil diameter; although higher densities are generated in the smaller diameter coil, the increased initial E_θ results in higher plasma column temperatures and since $\ell_{ab} \propto T_e^{3/2}/n_e^2$ the absorption length is not significantly altered by decreasing the coil diameter.

ACKNOWLEDGMENT

The author wishes to thank Dr. K. B. Freese for identifing the line spectra, W. T. Armstrong for his aid in the data reduction, E. L. Zimmermann for maintaining the experimental apparatus and S. E. Linzey for his technical assistance.

REFERENCES

1. K. F. McKenna, E. L. Zimmermann, and K. B. Freese, "Laser-Plasma Interaction in the Scylla I-C Theta Pinch," Third Topical Conference on Pulsed High-Beta Plasmas, Culham, England, Sept. 9-12, 1975.

2. T. M. York and K. F. McKenna, "Laser-Plasma Interactions in the Scylla I-C Experiment, Preliminary Analysis," Los Alamos Scientific Laboratory report LA-5957-MS (May 1975).

3. K. F. McKenna and T. M. York, "Plasma End Loss Studies in Scylla I-C," Los Alamos Scientific Laboratory report LA-6412-MS (August 1976).

4. G.B.F. Niblett and J. S. Green, "Radial Hydromagnetic Oscillations," Proc. Phys. Soc. LXXIV, 6, 737 (1962).

5. H.A.B. Bodin, T. S. Green, G.B.F. Niblett, N. J. Peacock, J.M.P. Quinn, J. A. Reynolds, "The Influence of Trapped Field on the Characteristics of a Magnetically Compressed Plasma," Nucl. Fusion, 2, 521 (1961).

6. L. Spitzer, *Physics of Fully Ionized Gases*, 2nd Ed., Interscience Pub., New York, (1962).

7. R. F. Gribble, W. E. Quinn, and R. E. Siemon, "Plasma Experiments with a Three-Meter θ Pinch," Phys. Fluids, 14, 2042 (1971).

8. K. S. Thomas, H. W. Harris, F. C. Jahoda, G. A. Sawyer, and R. E. Siemon, "Plasma Experiments on the Linear Scyllac Theta Pinch," Phys. Fluids, 17, 1314 (1975).

9. W. R. Ellis, J. P. Freidberg, R. E. Siemon, E. L. Zimmermann, in "LASL Controlled Thermonuclear Research Program, Los Alamos Scientific Laboratory report LA-5250-PR, 38 (June 1973).